CHIN. PHYS. LETT. Vol. 37, No. 8 (2020) 087503

Mode Structures and Damping of Quantized Spin Waves in Ferromagnetic Nanowires

Qingwei Fu(付清为)[1], Yong Li(李勇)[2], Lina Chen(陈丽娜)[1], Fusheng Ma(马付胜)[2], Haotian Li(李浩天)[1], Yongbing Xu(徐永兵)[3,4], Bo Liu(刘波)[5], Ronghua Liu(刘荣华)[1*], and Youwei Du(都有为)[1]

[1]*National Laboratory of Solid State Microstructures, School of Physics and Collaborative Innovation Center of Advanced Microstructures, Nanjing University, Nanjing 210093, China*

[2]*Jiangsu Key Laboratory of Opto-Electronic Technology, Center for Quantum Transport and Thermal Energy Science, School of Physics and Technology, Nanjing Normal University, Nanjing 210023, China*

[3]*York-Nanjing Joint Center (YNJC) for Spintronics and Nanoengineering, School of Electronics Science and Engineering, Nanjing University, Nanjing 210093, China*

[4]*Spintronics and Nanodevice Laboratory, Department of Electronics, University of York, York YO10 5DD, United Kingdom*

[5]*Key Laboratory of Spintronics Materials, Devices and Systems of Zhejiang Province, Hangzhou 311300, China*

(Received 25 April 2020; accepted 17 June 2020; published online 28 July 2020)

Magnonic devices based on spin waves are considered as a new generation of energy-efficient and high-speed devices for storage and processing of information. Here we experimentally demonstrate that three distinct dominated magneto-dynamic modes are excited simultaneously and coexist in a transversely magnetized ferromagnetic wire by the ferromagnetic resonance (FMR) technique. Besides the uniform FMR mode, the spin-wave well mode, the backward volume magnetostatic spin-wave mode, and the perpendicular standing spin-wave mode are experimentally observed and further confirmed with more detailed spatial profiles by micromagnetic simulation. Furthermore, our experimental approach can also access and reveal damping coefficients of these spin-wave modes, which provides essential information for development of magnonic devices in the future.

PACS: 75.40.Gb, 75.47.−m, 75.78.−n, 75.78.Cd DOI: 10.1088/0256-307X/37/8/087503

Spin waves (SWs), whose quanta are known as magnons, are dynamic eigenmodes that represent phase-coherent precession of microscopic vectors of magnetization in magnetically ordered media. SWs have the capability of carrying and processing information on the nanoscale with frequency ranging from microwave frequency to THz, making them a promising prospect for the development of ultralow energy, compact and high-speed magnonic devices.[1−5] To ultimately achieve the technological potential of magnonics, one has to design and build nanoscale functional magnonic devices for integration into the existing CMOS circuits, which gives rise to the prominent confinement effects generated by geometry or magnetic structure. Recently, the fundamental properties of dynamical spin excitation in various confined structures have been studied intensively by the optical and electrical methods.[6−8] The microscale metallic ferromagnetic wires (FWs), a potential waveguide/channel for magnonic logic devices, as the most basic confined structure, have attracted tremendous attention.[6,8−11] Although some models have been proposed to understand the spin waves confined by FWs,[8−10] there is still a lack of quantitative analysis of the excitation and spatial information of the distinct spin-wave modes and the corresponding damping properties, which have essential impacts on the performance of magnon-based devices. In addition, dependences of spin-waves damping on structure, material, and wave vector are also widely concerned in designs of magnonic devices.[12−16] Consequently, the clear identification of several dominated spin waves confined in FWs and the understanding of the properties of spin wave damping properties are necessary to address.

In this work, we quantitatively investigate the spin-wave excitation of transversely magnetized permalloy (Py) FWs by combining electrically ferromagnetic resonance (FMR) and nano-patterned coplanar waveguide (CPW) techniques. Besides the uniform FMR mode, three distinct spin-wave modes are experimentally observed in 2-μm-wide FWs under the transverse bias field geometry. They are identified as backward volume magnetostatic spin-wave (BVMSW)

Supported by the National Key Research and Development Program of China (Grant No. 2016YFA0300803), the Open Research Fund of Jiangsu Provincial Key Laboratory for Nanotechnology, the National Natural Science Foundation of China (Grant Nos. 11774150 and 11704191), and the Natural Science Foundation of Jiangsu Province (Grant Nos. BK20171026 and BK20170627).

*Corresponding author. Email: rhliu@nju.edu.cn

© 2020 Chinese Physical Society and IOP Publishing Ltd

modes, spin wave well (SWW) modes, and perpendicular standing spin-wave (PSSW) mode. SWW modes with several quantum numbers ($n = 1, 2, 3$) are strongly localized in two field-free boundary zones (FFBZs) of FWs by quantum well effect due to dipole field and edge effect, while the BVMSW modes extend to the full width of the FW. The mode-dependent damping properties of two former spin-wave modes are also quantitatively analyzed. Furthermore, our micromagnetic simulation quantitatively reproduces the main observed results, and meanwhile gives more detailed spatial profiles of SWW and BVMSW modes.

Figure 1(a) schematically shows the experimental setup of FMR. An array of 50-nm-thick Py wires were patterned on the S-pole of the CPW made of a 50-nm-thick gold layer. These Py wires have 80 μm length ($l = 80\,\mu$m) and 2 μm width ($w = 2\,\mu$m). The distance between the midpoints of two wires is 4 μm, where the inter dipole interactions are negligible. Figure 1(b) shows their scanning electron microscope (SEM) images. All differential FMR spectrum measurements were carried out with a home-made differential FMR measurement system combining the lock-in technique at room temperature. An ac Oersted field, to excite spin waves in a patterned Py wire array, was generated through the S-pole via connecting CPW with a microwave generator. The bias magnetic field was modulated by a pair of secondary Helmholtz coils powered by an alternating current source with 500 Hz [Fig. 1(a)].

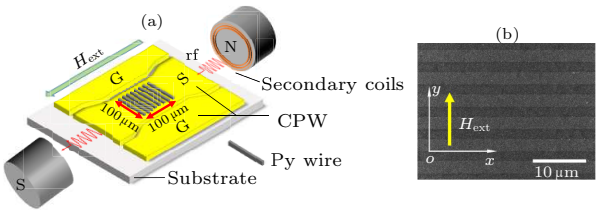

Fig. 1. (a) Schematic diagram of the FMR measurement setup and the coplanar waveguide (CPW). The applied in-plane magnetic field H_{ext} was along the CPW and perpendicular to Py wires. (b) SEM images of 50-nm-thick Py-wire array.

In a downscaled FWs, the geometric demagnetization effect dramatically affects the spatial distribution of magnetic moment, thus establishing a field-free boundary zone (FFBZ).[17–20] The size of the FFBZ is related to the total field including the applied external field and demagnetization field as follows:[21]

$$s = \frac{tM_s}{\pi H_0}, \tag{1}$$

where H_0 is the external applied magnetic field, s and t are the width and thickness of the FFBZ, respectively. Based on Eq. (1), the FFBZ can be devastated by a higher bias field, indicating that there is a distinct magnetodynamics in high and low field ranges.

To obtain the details of the spin excitation dynamics of the transversely magnetized nanowire, we first performed FMR measurements of the FW sample-1 at in a higher bias field range. The typical differential FMR spectrum with the primary peak corresponding to FMR mode and two secondary peaks at high fields is shown in the inset of Fig. 2(a). The two secondary peak are the quantized standing spin waves named BVMSW with different wave vectors $k = n\pi/w$ due to the quantum confinement effect along the wire width when the bias field is perpendicular to the wire.[12] In order to extract the resonance field and linewidth information of these modes, the differential spectra data was fitted with a differentiated function including the symmetric and anti-symmetric Lorentzian lineshape:

$$\frac{dP}{dH} = F_S \frac{4\Delta H(H - H_{res})}{[4(H - H_{res})^2 + (\Delta H)^2]^2} - F_A \frac{(\Delta H)^2 - 4(H - H_{res})}{[4(H - H_{res})^2 + (\Delta H)^2]^2}, \tag{2}$$

where F_S and F_A are the symmetric and anti-symmetric components of the derivative FMR spectra, respectively, H is the applied magnetic field, H_{res} and ΔH are the corresponding resonance field and linewidth of the excitations, respectively. Figure 2(a) shows the frequencies f versus resonance fields H_{res} dispersion relation of the primary FMR mode and the secondary modes. The former can be fitted well using the Kittel formula[22] with the parameters $M_S = 9.5$ kOe, as shown by the black line.

The dispersion relation is the indicator to identify the excitation spin-waves modes. Here we adopted the simplified model of the standing BVMSW modes pinned by the edges. In our studied FW system, the dispersion of dipole-exchange spin waves can be expressed as[21]

$$\left(\frac{\omega}{\omega_M}\right)^2 = \left(\frac{H_0}{M_s} + \frac{\langle H_{dy}\rangle}{M_s} + \Lambda^2 k^2\right)^2 + \left(\frac{H_0}{M_s} + \frac{\langle H_{dy}\rangle}{M_s} + \Lambda^2 k^2\right)\left(\frac{1 - e^{-k\Delta}}{k\Delta}\right), \tag{3}$$

where $\omega_M = \gamma M_S$, $\gamma/2\pi = 29$ GHz/T is the gyromagnetic ratio, Λ is the exchange length, H_0 is the resonance field, Δ is the FW sample thickness, k is the wave vector perpendicular to the FW, and $\langle H_{dy}\rangle$ represents the spatial average of the static dipole field weighted by the amplitude of the oscillating magnetization.[21,23] Fitting the experimental data of BVMSW modes with Eq. (3), we obtain the odd quantization indexes $n = 3$ for the first-order mode and $n = 5$ for the second-order mode, as represented in Fig. 2(a). The non-integer fitting parameter $n = 3.2$ is probably attributed to the edge inhomogeneity during the nanofabrication. The odd quantization index is owing to the edge pinning of the magnetization. Based on our calculation, the dipole field related

$\langle H_{dy}/M_S\rangle_{n=3.2}$ and $\langle H_{dy}/M_S\rangle_{n=5}$ of both BVMSW modes are -0.0072 and -0.0084, respectively, which is qualitatively consistent with the prior results reported by Bailleul *et al.*[21]

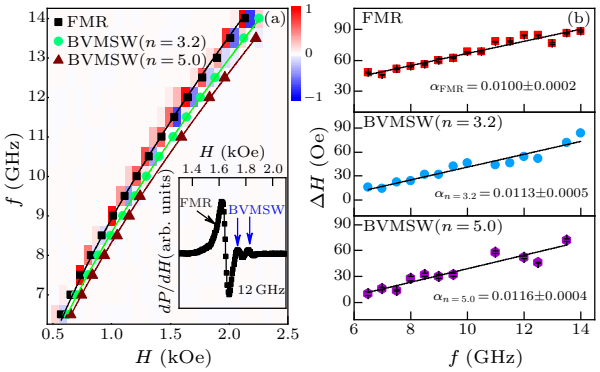

Fig. 2. Experimental spectra of the Py wire array in the high-field range. (a) Pseudocolor plot of the differential FMR spectra. The solid lines are the fitting curves using the Kittle formula. The inset is the representative FMR spectrum obtained at 12 GHz. (b) Frequency dependence of linewidth for FMR mode (upper panel), the fundamental (middle panel) and higher-order $n = 3$ (lower panel) of BVMSW modes. The solid line is a linear fitting, which can extract the corresponding damping constant α.

The damping constant is a crucial property of the spin excitation dynamics.[11–15,24,25] The effective spin damping α of the different spin-wave modes can be determined from frequency-dependent linewidth ΔH relation: $\Delta H = \Delta H_0 + \frac{4\pi\alpha f}{\gamma}$. Both the linewidth ΔH of FMR mode and BVMSW modes are displayed as symbols in Fig. 2(b). It should be noted that the linewidth of the standing BVMSW modes are smaller than the uniform FMR excitation, which arises from the coupling between the magnons and the RF driving field. The effective damping constants of different modes were determined by frequency-dependent linewidth ΔH relation, as shown in Fig. 2(b). For the uniform mode $k = 0$, the damping constant $\alpha_{FMR} = 0.0100 \pm 0.0002$ is the same as the previously reported results.[12] For the standing BVMSW modes with $k = 4.71$ and $7.85\,\mu m^{-1}$, the damping constants $\alpha_{n=3} = 0.0113 \pm 0.0005$ and $\alpha_{n=5} = 0.0116 \pm 0.0004$ have an enhancement of $\sim$10% compared to the uniform mode $k = 0$. Our results are compared with the case reported by Huo *et al.*,[12] where damping of the BVMSW mode was smaller than that of the uniform mode by 25% while consistent with the damping enhancement of the quantized spin wave reported by Li *et al.*[13] and Boone *et al.*[26] For the damping enhancement, two main mechanisms are generally accepted: spin current[14,24,27–29] and eddy current effects.[13,25,30–33] Nembach *et al.*[14] found that the enhanced damping of spin waves by spin current is proportional to the square of the wavenumber. Since some experiments suggested that Py films have a considered value of spin Hall effect due to spin–orbit coupling in the bulk of Py, a spin current would be generated by spin pumping mechanism in our Py wire system during the FMR spectrum measurement. This spin current can damp the spin-waves excitation. To quantitatively estimate damping enhancement by spin current, we can add a spin current related damping term α_{sc} in the LLG equation[24]

$$\alpha_{sc} = \eta k^2, \tag{4}$$

where η is the parameter of spin current-induced damping enhancement. We adopt the parameter $\eta = 0.16\,nm^2$ to estimate spin current-induced additional damping for our system. For the BVMSW mode with $k = 7.85\,\mu m^{-1}$, $\alpha_{sc} \cong 0.00001$, only 1‰ of the total damping constant obtained from our FMR data above is too small to cause 10% damping enhancement of the dipole-exchange dominated BVMSW modes. Now let us take account of the eddy current effect as the main contribution to the damping enhancement of the BVMSW modes. Since the eddy current related damping increases with the film thickness,[13] the Py nanowire with 50-nm thickness should have strong eddy current effects on the magnon damping enhancement. The corresponding spin-wave damping due to the eddy current can be quantitatively expressed by[25]

$$\alpha_{eddy} = \frac{C}{16}\frac{\gamma\mu_0^2 M_s \Delta^2}{\rho}, \tag{5}$$

where ρ is the resistivity of the sample, Δ is the thickness of the ferromagnetic wire and C is the eddy-current spatial distribution. Based on Eq. (5), one can have the relative damping $\alpha_{eddy} \cong 0.001$ with $C_{eff} = 0.7$, which agrees well with the damping enhancement of BVMSW modes observed in our experiments. Generally, eddy current would enhance the damping of all excited modes.[31] However, the eddy current-induced damping enhancement was inconsiderable for the uniform mode in our experiment, which was confirmed by performing additional FMR measurements on a 50-nm-thick Py film without the adjacent gold layer. Based on the results and analysis, we find that the eddy current effect dominates the damping enhancement of BVMSW modes.

As mentioned above, FWs could exhibit different dynamic behaviors as the FFBZ becomes predominant part with the bias field decreasing. Thus, we performed additional FMR measurements below 1.2 kOe (sample 2). Figure 3(a) shows the frequency vs field dispersion of several observed spin-waves extracted from the differential FMR spectra. The FMR mode is fitted well by the Kittel formula with the same parameters of the sample 1. The fundamental BVMSW mode ($n = 3$) was also observed above 0.6 kOe. Another higher frequency mode begins to appear below 0.25 kOe and has a very weak frequency dependence on the external bias field. These features indicate that

it is the PSSW mode.[6] More importantly, three other lower frequency modes were distinctly observed below the frequency of the BVMSW mode, as shown in Fig. 3(a). As discussed above, FFBZ would create a potential well and stabilize new-type standing spin-waves under a moderate external bias field. Because of the confining effect of FFBZ, the spin waves were quantized and defined as spin-wave well magnons (SWW-type magnons). To clarify the dynamics of the SWW-type modes, we quantitatively analyzed the dispersion relation between frequencies and bias fields. Since the dipole interaction dominates the FFBZs, we use the dipole model to analyze the SWW-type modes as[21]

$$\left(\frac{\omega_n}{\omega_{\rm M}}\right)^2 \frac{t+s}{s} = \beta\frac{H_0}{M_{\rm s}} + \delta\frac{H_0}{M_{\rm s}}\left[1-\left(1-\frac{n-\frac{1}{2}}{\nu}\right)^2\right] + \text{offset}. \tag{6}$$

The parameters $\beta = 0.94$, $\delta = 0.39$ and $\nu = 3.7$ are used in the fitting [Fig. 3(a)]. The anharmonicity parameter ν is close to 4, indicating that this potential well gives rise to four bound states for spin-waves excitation. Due to the intensity attenuation with the quantization index n increasing,[12,21] only three SWW modes were observed in our experiment, while all four modes were reproduced by the micromagnetic simulation [Figs. 4(h)–4(k)]. The dashed lines represent the best-fitting curves in Fig. 3(a). Approximately, the dipole model gives a quantitative description of SWW-type modes located at the edge of the FW, and their more spatial details will be provided in the simulation.

Similarly to the BVMSW modes, the damping properties of the SWW-type magnons were also analyzed and the damping constant were extracted as $\alpha_{n=1} = 0.006 \pm 0.001$, $\alpha_{n=2} = 0.006 \pm 0.002$ and $\alpha_{n=3} = 0.008 \pm 0.002$, as shown in Fig. 3(b). The mode-dependent damping reduces by ∼40%, 40%, and 20% for the fundamental, second and third-order SWW modes compared to the uniform FMR mode $\alpha_{\rm FMR} = 0.0100 \pm 0.0002$, respectively. Although it is unclear why $\alpha_{n=3}$ is larger than $\alpha_{n=1,2}$, the quantitative tendency consistently reveals that the damping constant of the localized SWW-type magnon is substantially smaller than the uniform mode. Many previous works also observed the reduction behavior of spin-waves damping.[6,12,14,16,33] Some suggested that the nonlinear effect could change the spin-wave properties when the spin waves are excited under a high-power external stimulating signal.[33] In our measurement, the applied microwave power is 15 dBm, which may cause a strong nonlinear effect of spin waves. Due to the nonlinear effect, the magnons of the system are redistributed, which results in less energy consumption for the excitation of the same energy magnons, and thus reduces the damping of localized magnons.[14,33] The different reductions for SWW modes with different k may originate from the diver relaxation rates for different modes.

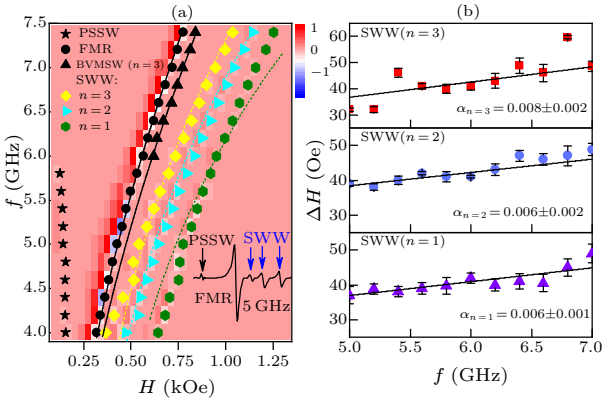

Fig. 3. Experimental spectra of the Py wire array in the low-field range. (a) Pseudocolor plot of the normalized differential FMR spectra. The symbols represent the resonance fields $H_{\rm res}$ of PSSW (star), FMR (circle), BVMSW (uptriangle) and SWW modes (square, right-triangle, and hexagon). (b) Frequency dependence of linewidth for the fundamental $n = 1$ (lower panel), the $n = 2$ (middle panel) and $n = 3$ (upper panel) of SWW mode. The solid line is the best linear fitting.

Since micromagnetic simulations can help us to obtain the detailed profiles of the magnetic dynamics of the microscale structures, we performed additional micromagnetic simulations based on the configuration of our devices using the MuMax package.[34] The size of the simulated Py stripe is 10 μm × 2 μm × 50 nm. The simulation parameters include the saturation magnetization $M_{\rm s} = 886\,{\rm kA/m}$, the exchange coefficient $A = 13 \times 10^{-12}\,{\rm J/m}$, the damping constant $\alpha = 0.001$ and the cell size 10 nm × 10 nm × 50 nm. Figure 4(a) shows the calculated dispersion relation, which qualitatively reproduces all the main characteristics of the results observed in our experiments. A typical spectrum calculated at bias field $H = 1.2\,{\rm kOe}$, including the primary FMR peak, BVMSW peak, and several SWW modes, is shown in the inset of Fig. 4(a). In addition, a weak Demon–Eshbach mode is also visible in our simulations. To get further insight into the dynamic modes observed in our experiments, we separately extracted the spatial distributions of different modes from the simulations, as shown in Fig. 4(c)–4(k). Figure 4(c) shows a uniform spatial intensity, indicating the FMR mode excitation. Figures 4(d) and 4(e) show the standing BVMSW with odd nodes $n = 3$ and 5, confirming our experimental observations. To obtain the dynamical properties of FFBZs, we also extracted the spatial profiles of the spin waves with low frequencies at a low field $H = 0.8\,{\rm kOe}$, as shown in Figs. 4(f)–4(k). Compared to the spectra excited at 2 kOe, we found that the excitation region of both FMR and BVMSW was forced to shrink to the center from the edges of the FW. Moreover, we found that the emerging several standing-type spin-

wave modes with much lower frequencies were localized in the edge regions of the FW [Figs. 4(h)–4(k)], which is consistent with the above discussion that the dipole-field-induced potential well in the FFBZs can facilitate another SWW-type mode under the moderated transverse magnetic field. The SWW-type mode with several quantization indexes ($n = 1, 2, 3, 4$) is also well consistent with our experimental results and the above quantitative analysis.

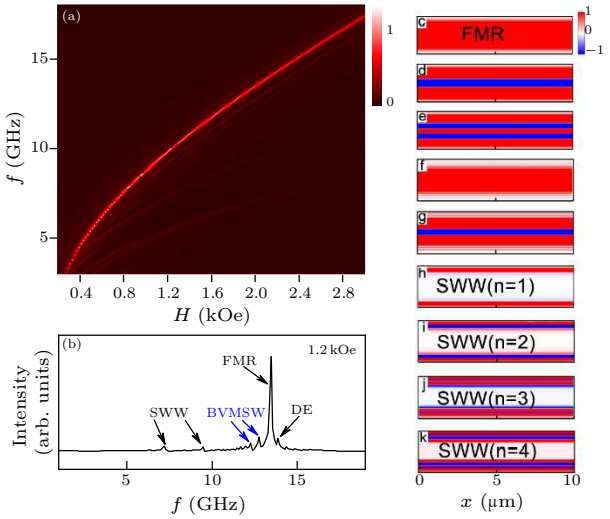

Fig. 4. Micromagnetic simulation results. (a) Pseudo-color plot of the field-dependent calculated spectra of the Py wire. (b) Representative spectrum calculated at bias field $H = 1.2$ kOe. (c)–(e) Spatial distributions of the normalized magnitude of magnetization for the uniform FMR (c) and the fundamental $n = 3$ (d) and higher-order $n = 5$ (e) of the standing BVMSW modes at 2.0 kOe, respectively. (f)–(k) Spatial distributions of FMR (f), BVMSW mode with $n = 3$ (g) and SWW modes with $n = 1$ (h), $n = 2$ (i), $n = 3$ (j) and $n = 4$ (k) at 0.8 kOe, respectively.

In summary, in a transversely magnetized microscale Py wire system, besides FMR mode, the odd BVMSW modes ($n = 3, 5$) are observed experimentally and well-identified by the simplified model of BVMSW. We find that the damping constant of the standing BVMSW modes has an enhancement ∼10% compared to that of the uniform FMR mode. Our analysis suggests that the current eddy mechanism dominates the damping enhancement of the standing BVMSW. Additionally, our quantitative analysis and simulation results also indicate that the experimentally observed three abnormal modes with much lower frequencies at low fields belong to a new-type SWW mode localized in the two FFBZ edges of the ferromagnetic wire and can be suppressed completely by increasing the external bias field. Our simulations also provide a more detailed spatial information about the BVMSW and SWW modes observed in our experiments, which enables us to reach a deep understanding of its dynamic properties. Our results make further insight into the complexity of the dynamical magnetization states in microscale confined FWs, which offers valuable information regarding the excitation of spin waves for the development of magnonic devices.

References

[1] Wagner K *et al.* 2016 *Nat. Nanotechnol.* **11** 432
[2] Lan J, Yu W, Wu R and Xiao J 2015 *Phys. Rev. X* **5** 041049
[3] Min R *et al.* 2009 *Chin. Phys. B* **18** 2006
[4] Zhang G F *et al.* 2015 *Chin. Phys. B* **24** 097503
[5] Li S F *et al.* 2014 *Chin. Phys. Lett.* **31** 017502
[6] Duan Z *et al.* 2014 *Phys. Rev. B* **90** 024427
[7] Rana B and Otani Y 2018 *Phys. Rev. Appl.* **9** 014033
[8] Bocklage L *et al.* 2014 *J. Phys.: Condens. Matter* **26** 266003
[9] Park J P *et al.* 2002 *Phys. Rev. Lett.* **89** 277201
[10] Jorzick J *et al.* 1999 *Phys. Rev. B* **60** 15194
[11] Purnama I, Moon J H and You C Y 2019 *Sci. Rep.* **9** 13226
[12] Huo Y *et al.* 2016 *Phys. Rev. B* **94** 184421
[13] Li Y and Bailey W E 2016 *Phys. Rev. Lett.* **116** 117602
[14] Nembach H T, Shaw J M, Boone C T and Silva T J 2013 *Phys. Rev. Lett.* **110** 117201
[15] Shaw J M, Silva T J, Schneider M L and McMichael R D 2009 *Phys. Rev. B* **79** 184404
[16] de Loubens G *et al.* 2007 *Phys. Rev. Lett.* **98** 127601
[17] Jorzick J *et al.* 2002 *Phys. Rev. Lett.* **88** 047204
[18] Bayer C, Demokritov S O, Hillebrands B and Slavin A N 2003 *Appl. Phys. Lett.* **82** 607
[19] McMichael R D and Maranville B B 2006 *Phys. Rev. B* **74** 024424
[20] Bryant P and Suhl H 1989 *Appl. Phys. Lett.* **54** 2224
[21] Bailleul M, Höllinger R and Fermon C 2006 *Phys. Rev. B* **73** 104424
[22] Kittel C 1948 *Phys. Rev.* **73** 155
[23] Guslienko K Y, Chantrell R W and Slavin A N 2003 *Phys. Rev. B* **68** 024422
[24] Zhang S and Zhang S S L 2009 *Phys. Rev. Lett.* **102** 086601
[25] Schoen M A W *et al.* 2015 *Phys. Rev. B* **92** 184417
[26] Boone C T *et al.* 2009 *Phys. Rev. Lett.* **103** 167601
[27] Wong C H and Tserkovnyak Y 2009 *Phys. Rev. B* **80** 184411
[28] Tserkovnyak Y, Hankiewicz E M and Vignale G 2009 *Phys. Rev. B* **79** 094415
[29] Foros J, Brataas A, Tserkovnyak Y and Bauer G E W 2008 *Phys. Rev. B* **78** 140402
[30] Pincus P 1960 *Phys. Rev.* **118** 658
[31] Kalinikos B A and Slavin A N 1986 *J. Phys. C* **19** 7013
[32] Almeida N S and Mills D L 1996 *Phys. Rev. B* **53** 12232
[33] de Loubens G, Naletov V V and Klein O 2005 *Phys. Rev. B* **71** 180411
[34] Vansteenkiste A *et al.* 2014 *AIP Adv.* **4** 107133